Structure-based Inhibitor Design for an Enzyme That Binds Different Steroids

A POTENT INHIBITOR FOR HUMAN TYPE 5 17β-HYDROXYSTEROID DEHYDROGENASE*[s]

Wei Qiu[1,2], Ming Zhou, Mausumi Mazumdar[1], Arezki Azzi, Dalila Ghanmi, Van Luu-The, Fernand Labrie, and Sheng-Xiang Lin[3]

From the Canadian Institutes of Health Research Group in Molecular Endocrinology, Laval University Medical Center, Centre Hospitalier de Universités de Québec and Laval University, Quebec G1V 4G2, Canada

Human type 5 17β-hydroxysteroid dehydrogenase plays a crucial role in local androgen formation in prostate tissue. Several chemicals were synthesized and tested for their ability to inhibit this enzyme, and a series of estradiol derivatives bearing a lactone on the D-ring were found to inhibit its activity efficiently. The crystal structure of the type 5 enzyme in complex with NADP and such a novel inhibitor, EM1404, was determined to a resolution of 1.30 Å. Significantly more hydrogen bonding and hydrophobic interactions were defined between EM1404 and the enzyme than in the substrate ternary complex. The lactone ring of EM1404 accounts for important interactions with the enzyme, whereas the amide group at the opposite end of the inhibitor contributes to the stability of three protein loops involved in the construction of the substrate binding site. EM1404 has a strong competitive inhibition, with a K_i of 6.9 ± 1.4 nM, demonstrating 40 times higher affinity than that of the best inhibitor previously reported. This is observed despite the fact that the inhibitor occupies only part of the binding cavity. Attempts to soak the inhibitor into crystals of the binary complex with NADP were unsuccessful, yielding a structure with a polyethylene glycol fragment occupying the substrate binding site. The relative crystal packing is discussed. Combined studies of small molecule inhibitor synthesis, x-ray crystallography, enzyme inhibition, and molecular modeling make it possible to analyze the plasticity of the substrate binding site of the enzyme, which is essential for developing more potent and specific inhibitors for hormone-dependent cancer therapy.

According to the American Cancer Society, prostate cancer is the most common malignant tumor, excluding skin cancers, in American men. It is estimated that ~232,090 new cases of prostate cancer will be diagnosed in the US during 2005 with 30,350 deaths (www.cancer.org). The growth and function of the prostate is dependent on androgens, which play important roles in the pathogenesis of prostate cancer (1). Androgen withdrawal triggers the programmed cell apoptosis in both normal prostate glandular epithelia and androgen-dependent prostate cancer cells. Androgen-independent prostate cancer cells do not initiate the programmed cell death pathway upon androgen withdrawal; however, they do retain the cellular machinery necessary to activate the apoptotic cascade when sufficiently damaged by exogenous agents (2).

In prostate cancer, the balance between cell proliferation and programmed cell death is lost, thus more cell proliferation results in net cell growth. An important finding in prostate cancer research is that ~50% of dihydrotestosterone, the most potent natural androgen, remains in the prostatic tissue of patients who have undergone surgical or chemical castration (3). In fact, prostatic tissue is able to efficiently transform the inactive adrenal steroid precursor dehydroepiandrosterone, into the active androgen dihydrotestosterone, in a new androgen biosynthetic pathway in which human type 5 17β-hydroxysteroid dehydrogenase (17β-HSD5)[4] is involved (4–7). In practice, hormonal therapy with combined androgen blockade could lead to even longer term control of localized prostate cancer (8, 9).

17β-HSD5 has also been known as type 2 3α-HSD (10), prostaglandin 11-ketoreductase (prostaglandin F synthetase) (11), and dihydrodiol dehydrogenase (12). It is a member of the aldo-keto reductase (AKR) family with a designated name of AKR1C3 (13, 14) and was first cloned from human prostate and placenta cDNA libraries (10, 15). It has been proven that this enzyme has a relatively high 17β-HSD activity that transforms Δ4-androstene-3,17-dione (4-dione, a weak androgen) to testosterone (a potent androgen). This enzyme has been immunocytochemically localized in human prostate tissues, and it has been proposed to contribute to local androgen formation in prostate (4–6, 16, 17). The enzyme conformational change during 4-dione to testosterone conversion was demonstrated by the first crystal structures of 17β-HSD5 in complex with

either 4-dione or testosterone (18, 19). The 11-ketoreductase activity of this enzyme has also been studied in association with prostaglandin D2 and some inhibitors (20, 21). Blockade of this enzyme could lead to the activation of a nuclear receptor (peroxisome proliferator-activated receptor-γ), which induces cell differentiation, and results in apoptosis in many cell types and cancers (22, 23).

The gene that encodes 17β-HSD5 was assigned to human chromosome bands 10p15 and p14 (24). 17β-HSD5 mRNA was also reported to be expressed in prostate cancer tissues (25). In a recent study, 17β-HSD5 immunoreactivity was detected in 77% of carcinoma cells from prostate cancer tissues and was positively associated with the clinical stage of the disease (17). This provides some evidence that 17β-HSD5 may possibly be involved in the increase of the local concentration of testosterone. Both reductive and oxidative 17β-HSD activities are present in prostate tissue (26, 27), assumed by different members of the 17β-HSD family members. Using the androgen-sensitive LNCaP prostate cancer cell line as a cell model to study the progression of prostate cancer, it has been reported that substantial changes in androgen and estrogen metabolism occur in the cells during this process. A remarkable decrease in the oxidative 17β-hydroxysteroid dehydrogenase activity was seen, whereas the reductive activity (including 17β-HSD5 and 17β-HSD7) seemed to increase (28).

It has also been reported that 17β-HSD5 mRNA expression was significantly higher in breast tumor specimens than in normal tissue after analysis of 794 breast carcinoma specimens by tissue microarray and normal histologic sections (29). This suggests that the ability of 17β-HSD5 to regulate estrogen metabolism may play an important role in breast cancer development. It is also interesting to point out that 17β-HSD5 plays an important site-specific role in androgen generation in adipose tissue in women with simple obesity (30).

Due to the importance of this enzyme, not only in prostate cancer research but also in other hormone-related diseases, the design of an inhibitor targeting this key enzyme has been widely pursued (31–35). The crystal structure of 17β-HSD5 is a necessary prerequisite for structure-based drug design. The enzyme was first crystallized in our laboratory (36), and structures in complex with testosterone or 4-dione were determined (18, 19). To date, eight crystal structures of AKR1C3 in different complexes have been published (18, 20, 21). The plasticity of its substrate binding site in accommodating different ligands and its importance in hormone-related diseases led us to investigate further the structure-function relationships of this enzyme. The functional plasticity of the AKR1C3 as well as 1C1 and 1C2 enzymes has been discussed by Penning and colleagues previously (37).

Being aware that any subtle difference at the active site could be important for structure-based inhibitor design, we have studied the active site of the enzyme in detail by comparing the different docking properties of various inhibitors and ligands in the crystallographic structures. In this study, we report the crystal structure of 17β-HSD5 in complex with a potent inhibitor EM1404 and another structure with a segment of polyethylene glycol (PEG) made from 6 ethylene glycol units ($C_{12}H_{25}O_6$) bound in the active site. Enzyme inhibition by

EM1404 was also studied, and the comparison with other inhibitors has been discussed. Furthermore, we intended to explore the interactions between this potent inhibitor and its target enzyme, 17β-HSD5, and to provide suggestions for the improvement of inhibitor design based on the crystal structure.

MATERIALS AND METHODS

Purification and Crystallization—Human 17β-HSD5-glutathione S-transferase was overexpressed in *Escherichia coli* and purified by glutathione S-transferase affinity column and a Blue Sepharose column as described previously (36). After purification the protein was kept in potassium phosphate stock buffer of pH 7.5, in the presence of 10 mM K_2HPO_4, 1 mM EDTA, 1 mM dithiothreitol, 0.05% decylmaltoside, 1.2 mM NADP. The glutathione S-transferase tag was cleaved by overnight incubation at 4 °C with Thrombin protease. EM1404 was co-crystallized with 17β-HSD5 and NADP. Due to the low solubility of EM1404, it was first dissolved in 100% Me_2SO to a concentration of 25 mM and then diluted in 100% ethanol to a final concentration of 2.5 mM as a stock solution. It was added to protein-NADP complex solution (~2 μl of this stock solution into 2 ml of total mixture volume) to reach a final concentration of 2.5 μM. The mixture was then concentrated 10 –20 times before being diluted to ~2 ml by adding the same stock buffer mentioned above. Additional EM1404 was added once more, which could be then dissolved (see "Discussion"). The same concentration-dilution procedure was repeated to saturate the enzyme substrate binding site by the inhibitor. The protein was finally concentrated to ~10 –15 mg/ml. The co-crystallization condition of the EM1404 ternary complex has been refined from the former conditions crystallizing testosterone and 4-dione complexes (36). The reservoir solution contained 100 mM sodium citrate, pH 5.6, 0.24 M ammonium acetate, and 30% PEG 4000.

Human 17β-HSD5·NADP crystals were obtained at room temperature using the hanging-drop vapor diffusion method by mixing equal volumes of protein and a reservoir solution of 30% PEG 4000, 0.1 M sodium citrate, pH 5.6, 0.24 M ammonium acetate. During our first attempts, 17β-HSD5·NADP (final enzyme concentration 330 μM in the crystallization drop after equilibrium) binary complex crystals were soaked with repeated additions of EM1404 (final inhibitor concentration 560 μM), and similar crystal space groups were obtained (Table 1)

Data Collection and Processing—Both datasets of 17β-HSD5·EM1404·NADP and 17β-HSD5·PEG fragment·NADP were collected at the X-8C beamline in National Synchrotron Light Source, Brookhaven National Laboratory. Datasets were processed using the Mosflm (39) and HKL packages (40). The processing statistics data are given in Table 1.

Structure Solution and Refinement—The initial phases of 17β-HSD5·EM1404·NADP was obtained from a molecular replacement method using the EPMR program (41). A data set from 15 to 4 Å resolution was used in molecular replacement. The coordinates of the protein structure from the 17β-HSD5-testosterone-NADP complex in the P21 space group were used as the starting model. A correlation coefficient factor of 0.568 and an R-factor of 41.9% were obtained before any refinement. The initial phases of 17β-HSD5·PEG·NADP were obtained using a similar method.

TABLE 1

Data collection and refinement statistics of crystal structures of 17β-HSD5·EM1404·NADP and 17β-HSD5·PEG·NADP

	17β-HSD5·EM1404·NADP	17β-HSD5·PEG·NADP
Data processing statistics		
PDB code	1ZQ5	2FGB
Space group	P212121	P212121
Unit cell (Å)	a = 55.35, b = 62.78, c = 95.97	a = 55.52, b = 61.65, c = 95.12
Resolution range (Å)	29.8-1.30	47.6-1.35
Highest shell range (Å)	1.37-1.30	1.38-1.35
Total reflections	251,431 (23,897)[a]	220,439 (7,354)[a]
Unique reflections	79,292 (10,401)	68,648 (3,474)
Mosaicity (°)	0.32	0.38
Multiplicity	3.2 (2.3)	3.2 (2.1)
Completeness (%)	95.9 (87.0)	94.4 (65.2)
R_{merge} (%)[b]	5.4 (42.4)	6.5 (47.5)
Mean(I)/σ(I)	11.9 (2.1)	9.6 (2.0)
Refinement statistics		
Reflections	75,293	68,644
Resolution range (Å)	29.8-1.30	47.6-1.35
Highest shell range (Å)	1.33-1.30	1.38-1.35
R_{cryst} (%)[c]	18.1 (30.0)	17.2 (25.9)
R_{free} (%)	19.7 (35.4)	19.0 (29.7)
Average B-value (A2)		
Protein	11.51	15.5
Ligand	8.44	12.5
Water	24.77	26.9
Root mean square deviation from ideality		
Bonds (Å)	0.008	0.007
Angle (°)	1.332	1.255
Ramachandran plot (% residue in CORE)	91.8	93.2
Model content	321 residues, 315 H$_2$O, 1 EM1404, 1NADP, and 1 acetate	323 residues, 402 H$_2$O, 1 PEG, 1 NADP, and 1 acetate

[a] Statistics of the highest resolution shell are shown in parentheses.

[b] $R_{merge} = \Sigma_{hkl}\Sigma_j |I_j(hkl) - \langle I(hkl)\rangle| \Sigma_{hkl}\Sigma_j |I_j(hkl)|$, where $I_j(hkl)$ and $\langle I(hkl)\rangle$ are the intensity of measurement j and the mean intensity for the reflection with indices hkl, respectively.

[c] R_{cryst} and $R_{free} = \Sigma_{hkl}|F_{calc}(hkl) - |F_{obs}(hkl)|\Sigma_{hkl}|F_{obs}|$, where the crystallographic and free R-factors are calculated, including and excluding refined reflections, respectively. The R_{free} reflections set constituted 5% of the total number of reflections.

Starting from the molecular replacement model, the programs Resolve (42) and Refmac from the CCP4 package (43) were used to improve phases using a statistical density modification method. Rigid body refinement was done with data from 29 to 3.0 Å resolution. Automatic model rebuilding was carried out based on a prime-and-switch composite omit map to reduce any model bias due to refinement. Multiple refinement cycles were carried out using the program Refmac, and model building was done by the Coot program (44) based on sigma-A weighted $2F_o - F_c$ electron density maps. The last refinement steps were done with data from 29 to 1.30 Å resolution. The inhibitor position was very clear in the substrate binding site from the electron density maps. An acetate molecule was also identified near the substrate and cofactor binding sites and was induced during the co-crystallization (see above). The program Coot was also used to add water into the model. In the final model, 356 water molecules were included with good hydrogen bonding geometry. Both structures have been deposited in the PDB, the ID for 17β-HSD5·EM1404·NADP structure is 1ZQ5, while that for 17β-HSD5·PEG fragment·NADP is 2FGB.

Inhibition Study—A radioactive assay was used for the enzyme kinetics in the presence of EM1404 at different concentrations for its K_i determination. Purified 17β-HSD5, freshly frozen at −80 °C in small aliquots until use, has demonstrated very good reproduction of steady-state kinetics. The reactions were carried out in the presence of an excess of NADP (200 μM) at pH 7.5 and 37 ± 0.5 °C. The K_m for testosterone oxidation in the absence of EM-1404, and four apparent K_m values in the presence of 1, 3, 10, and 25 nM EM-1404, were determined.

Reactions were initiated by the addition of enzyme sample to a final concentration of 200 nM in the reaction mixture, aliquots of the reaction mixture were taken, and the reaction was stopped at different time intervals by extracting the steroids with 2.5× vol. of diethyl ether. The steroids were extracted, separated by TLC migration in 80% toluene and 20% acetone for a 10-cm distance, and analyzed by phosphorimaging. Initial velocities were measured with <5% substrate consumption. The experiments were repeated with different concentrations of testosterone ranging from 0.8 to 10 μM. To obtain an optimal signal, larger reaction mixture volumes were used for low substrate concentrations (*i.e.* 3-ml reaction mixtures for 0.8 μM testosterone, 2 ml for 1.8 μM, 1 ml for 4 μM, and 0.5 ml for 10 μM). All experiments were performed in duplicate. IC$_{50}$ values indicated the inhibitor concentration leading to 50% inhibition of the enzyme activity under the experimental conditions described in Ref. 34.

The values were calculate using Equation 1,

$$1/v = K_m/V_{max} \cdot (1 + [I]/K_i) \cdot 1/[S] + 1/V_{max} \qquad \text{(Eq. 1)}$$

where v is the initial velocity in the presence of different substrate concentrations, V_{max} is the maximum velocity, and [S] and [I] are the substrate and inhibitor concentrations (48).

The respective apparent K_m values in the presence of different inhibitor concentrations were then plotted *versus* these concentrations as shown by the *inset* of Fig. 5, the slope of which defines K_m/K_i (48), based on the linear regression of Equation 2.
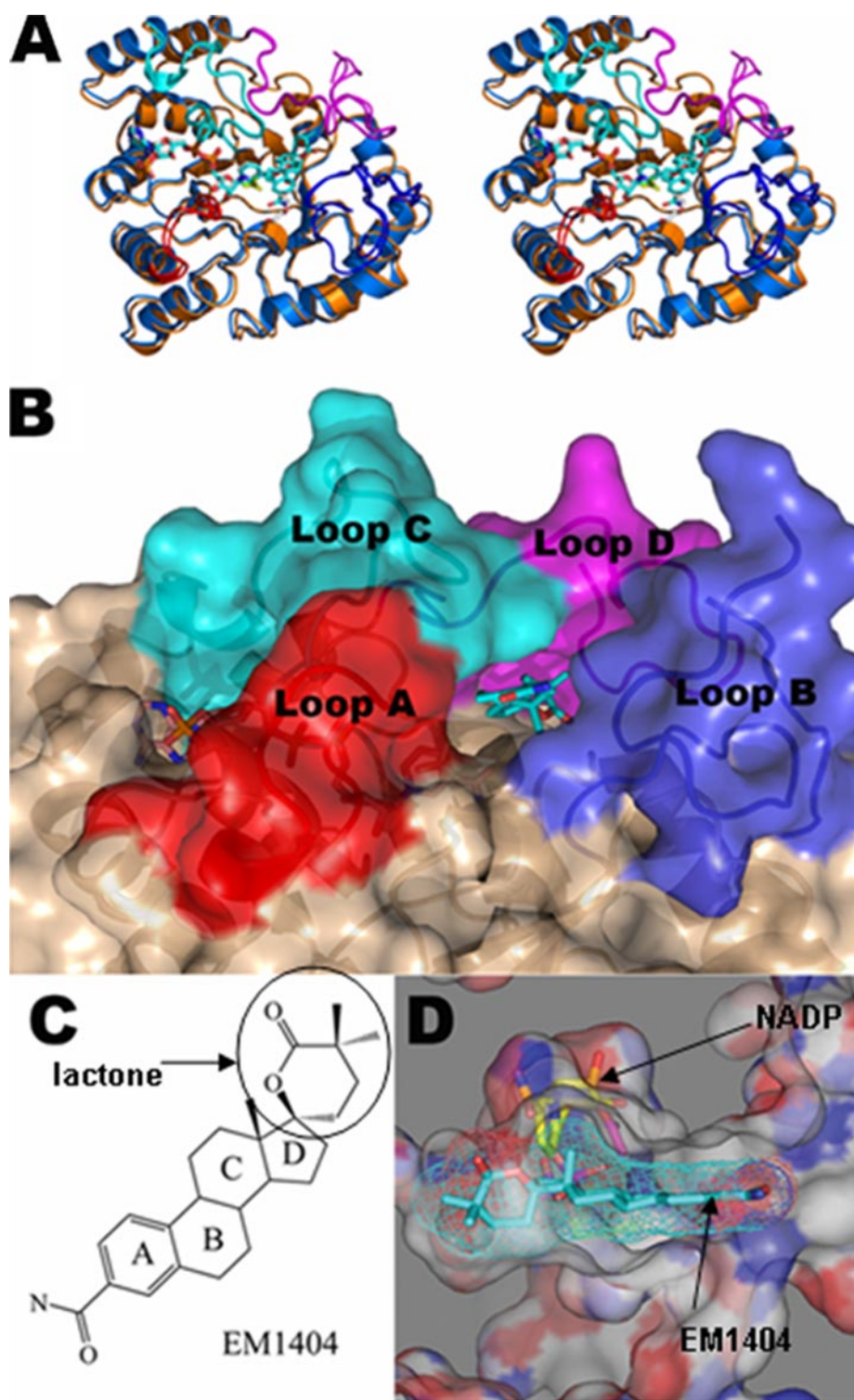
$$K_{mapp} = K_m(1 + [I]/K_i) \qquad \text{(Eq. 2)}$$

FIGURE 1. *A*, schematic representation of 17β-HSD5·EM1404·NADP (in *blue*, ID: 1ZQ5) and 17β-HSD5·PEG·NADP (*orange*, ID: 2FGB) structures. Four large loops, namely loop-A (24–33, *red*), loop-B (117–143, *blue*), loop-C (217–238, *cyan*), and loop-D (301–323, *magenta*), form the substrate and cofactor binding sites with modest movements. *B*, surface representation of four large loops form the substrate binding sites of EM1404. The *color scheme* is kept the same as in *panel A* for these loops; *C*, chemical structure of inhibitor EM1404: it is composed of an estradiol core, a lactone ring near the D-ring and an amide group at the A-ring; *D*, docking of EM1404 in its binding site. The *wall* around the middle portion of the binding pocket is lined with hydrophobic residues Leu-54, Trp-86, Trp-227, Phe-306, and Phe-311. The figures for the chemical structure of EM1404 here as well as other inhibitors shown in Figs. 5 and 8 were generated using ChemDraw (www.cambridgesoft.com). Other figures in this report were created using PyMOL (www.pymol.org) except for those indicated.

Molecular Dynamics Simulation— The simulations were based on the crystal structure for the complex EM1404 and the docked structure for the complex with the newly proposed inhibitor (Fig. 8*C*). MD simulations were performed with the program GROMACS (www.gromacs.org) version 3.3.1 (details are in the supplemental material). The GROMACS forcefield parameters were employed for the simulations.

RESULTS

Overall Structure—The inhibitor EM1404 (3-carboxamido-1,3,5-(10)-estratrien-17(*R*)-spiro-2′-(5′, 5′-dimethyl-6′-oxo)tetrahydropyran, $C_{25}H_{30}O_3N$, Fig. 1*A*) was first obtained from a chemical screen (34) where it was shown to have an IC_{50} (see definition in method) of 3.2 ± 1.5 nM, the best among the inhibitors designed for 17β-HSD5. The strong affinity of EM1404 is further proven in the inhibition mechanism study below. The ternary complex structure of 17β-HSD5·EM1404·NADP was determined by molecular replacement using a searching model obtained from the 17β-HSD5·testosterone·NADP complex (18). Its overall structure is similar to the other crystal forms (19–21), with an $(\alpha/\beta)8$ triose-phosphate isomerase barrel motif, a typical structure of the aldoketo reductase family. Four large loops, namely loop-A (24–33), loop-B (117–143), loop-C (217–238), and loop-D (301–323), contribute to form the substrate/inhibitor and cofactor binding sites (Figs. 1 and 2*B*). The final R_{cryst} and R_{free} values for this ternary complex were 18.2% and 19.8%, respectively, with 91.8% of the residues located in the most favored region of the Ramachandran plot (refer to PDB ID 1ZQ5). The final model includes residues 5–321 with clear electron density allowing the interpretation of most amino acids, the NADP cofactor, the EM1404 inhibitor, one acetate molecule, and 356 water molecules. However, it should be noted that residues 131–133 have no
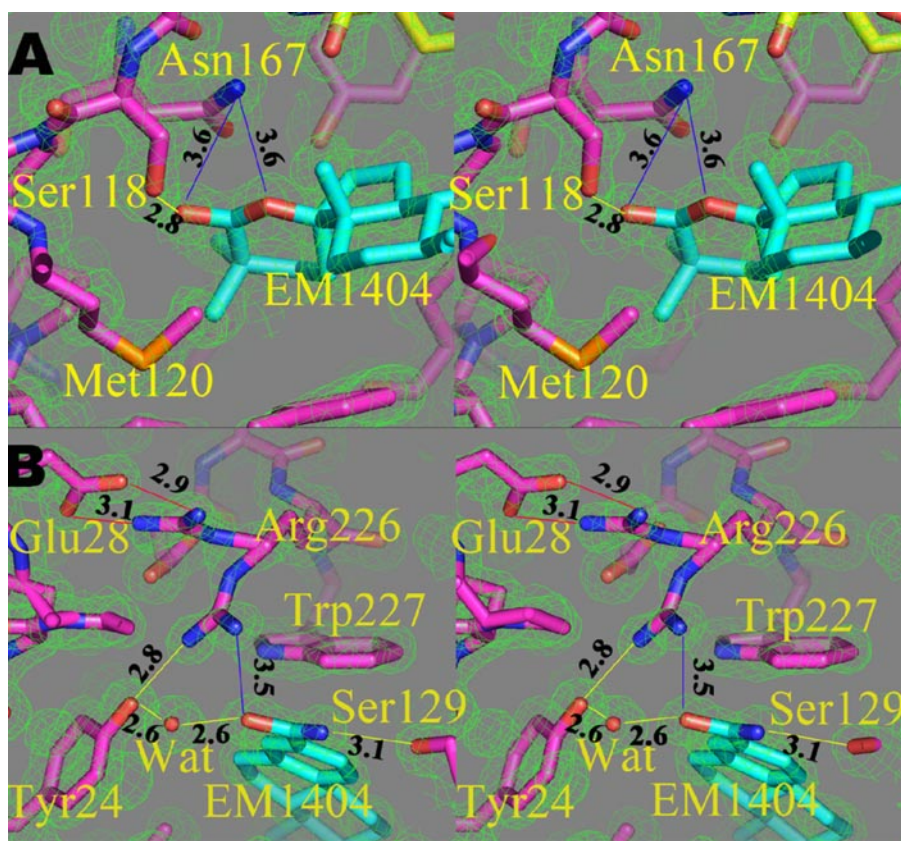
FIGURE 2. **17β-HSD5-EM1404 interactions.** Lactone ring accounts for the strong interaction between the EM1404 and 17β-HSD5. *A*, the carbonyl oxygen in the lactone ring forms a strong hydrogen bond with Ser-118 hydroxyl (2.8 Å). The side chain of Asn-167 has good Van der Waals contact with the lactone ring. The two methyl groups at the 3-carbon position in the lactone ring also show strong Van der Waals interactions with enzyme residues nearby and stabilize the conformation of the inhibitor. *B*, the nitrogen atom of the amide group of EM1404 forms a hydrogen bond to the Ser-129 hydroxyl (3.1 Å), which helps to stabilize loop-B; the oxygen atom of the amide group forms another water-mediated hydrogen bond with Tyr-24. It is of interest to note that the side chain of Arg-226 has two conformations: in one conformation, it forms two salt bridges with Glu-28, in another form, it forms a hydrogen bond with Tyr-24 (2.8 Å) and good Van der Waals contact with amide group of EM1404. Salt bridges have been marked in *red*, weak interactions in *blue*, and hydrogen bonding in *yellow*.

increased hydrogen bonding and hydrophobic interactions described below. The wall around the middle portion of the binding pocket is lined with some hydrophobic residues, which form a cavity complementary to the shape of EM1404. In particular, the steroid core of EM1404 is almost parallel to the side chain of Trp-227 with an interplanar distance of 3.4 Å. Trp-227, Phe-306, and Phe-311 are the three key residues that accommodate the docking of different ligands (see "Discussion"). It should be mentioned that Trp-227 and Phe-311 are highly conserved residues among AKR family members (see Fig. 6).

Potential hydrogen bonding partners from the enzyme are located either at the base or at the entrance of the binding pocket and include Tyr-24, Ser-118, Ser-129, Asn-167, and Arg-226. More number of hydrogen bonds and hydrophobic interactions were identified between the inhibitor EM1404 and 17β-HSD5 than those found in the enzyme-testosterone and enzyme-(4-dione) complexes. The 2′-carbonyl oxygen in the lactone ring forms a strong hydrogen bond with Ser-118 hydroxyl (2.8 Å) and another weak interaction is seen with Asn-167 side-chain amine

electron density and are thus presumed to be disordered. After the initial refinement, the $F_o - F_c$ electron density map showed unambiguous density for the inhibitor EM1404 at the substrate binding site. The atomic position of EM1404 was further refined with an average *B*-factor of 10.5 Å^2, whereas the average *B*-factor for the protein is 11.5 Å^2. The *B*-factor is significantly higher in the loop regions as compared with the overall protein. The maximum *B*-factor is observed in most structures for loop-B followed by loop-A (see supplemental materials).

Structure of the Inhibitor Binding Pocket—As shown in Fig. 1*C*, the inhibitor EM1404 consists of a steroid core (estradiol), a lactone ring, and an amide group. In the substrate binding site, the lactone ring of EM1404 is located at the base of the substrate binding site, whereas the amide group is oriented toward the surface of the enzyme. The EM1404 binding pocket is ~17 Å deep and has an elliptical shape with a short axis of 8 Å. The volume of the binding pocket is 949 Å^3, and the volume of EM1404 is 404 Å^3 in this complex. Despite the fact that the inhibitor occupies only part of the binding cavity, the inhibitor demonstrates high affinity at nanomolar levels (see "17β-HSD5 inhibition by EM1404"), which is likely contributed by the

group (3.6 Å, Fig. 2*A*). The 1′-oxygen in the lactone ring also forms a weak interaction with Asn-167 side chain amine group (3.6 Å). The two-methyl groups at the 3-carbon position in the lactone ring also show strong Van der Waals interactions with enzyme residues nearby and stabilize the conformation of the inhibitor. The lactone ring of EM1404 forms a strong network of hydrophobic interactions with the side chains of Met-120, Asn-167, Phe-306, Phe-311, Tyr-317, Pro-318, and Tyr-319. These residues, as well as Ser-118 and Tyr-216, form a compact binding pocket at the bottom of the substrate binding site that adapts well to the lactone ring of EM1404. The above-mentioned hydrogen bonds anchor the inhibitor firmly onto the bottom of the active site.

At the amide group of the A-ring end of EM1404, three more hydrogen bonds were located: the first is between the nitrogen atom of the amide group of EM1404 to the Ser-129 hydroxyl (3.1 Å), which helps to stabilize loop-B; the second is between the oxygen atom of the amide group to a water molecule (2.5 Å), which also forms a second hydrogen bond to the Tyr-24 hydroxyl (2.6 Å) (from loop-A), thus bridging the inhibitor and the enzyme; the third is between the oxygen atom of the amide group and Arg-226 NH$_2$ (3.4 Å) stabilizing loop-C. It is inter-
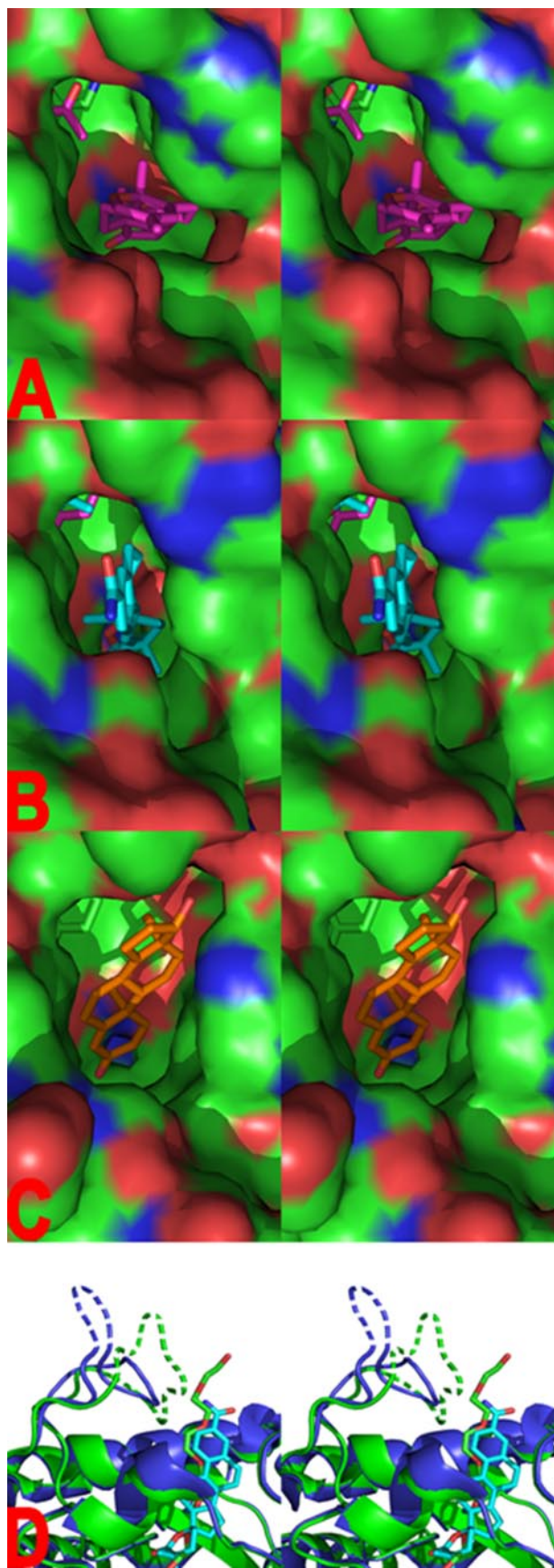
FIGURE 3. **The different orientations of ligand docking in the substrate binding site.** *A*, 17β-HSD5·4-dione·NADP structure, 4-dione is colored in *magenta*; *B*, 17β-HSD5·EM1404·NADP, EM1404 is colored in *cyan*;

esting to point out that Arg-226 has two conformations at the end of its side chain, as shown in Fig. 2*B*. Both conformations have similar occupancies based on the refinement. In one conformation, the two Arg-226 amine groups form a pair of hydrogen bonds with Tyr-24 hydroxyl and the EM1404 amide group oxygen. In the other conformation, these two amine groups form a pair of hydrogen bonds with the Glu-28 carboxyl group (from loop-A).

Comparison of the Enzyme-binding Site in Complex with Different Ligands—The structures were superimposed based on the eight beta strands in the center, which are the most structurally conserved element among all the structures. After superimposing all the available crystal structures for 17β-HSD/AKR1C3 we discovered that the overall structures are very similar despite the fact that they bind to ligands of different sizes, ranging from one as small as 2-methyl-2,4-pentanediol ($C_6H_{14}O_2$) to one as large as 2-(3,4-dihydroxyphenyl)-5,7-dihydroxy-4-oxo-4h-chromen-3-yl-6-*o*-(6-deoxy-α-mannopyranosyl)-β-ᴅ-glucopyranoside (rutin, $C_{27}H_{30}O_{16}$). The major deviations are located in the loops that form the substrate binding site (Fig. 3) and are mainly related to the side-chain conformational changes within three residues, namely Trp-227, Phe-306, and Phe-311. When we superimposed the structures of 17β-HSD5·EM1404·NADP and 17β-HSD5·PEG-fragment·NADP (see description below), residue Phe-311 Cα on loop-D moves by 1.90 Å, residue Arg-226 on loop-C is displaced by 0.62 Å, and residue Pro-27 on loop-A moves by 1.12 Å. In the superimposed structures of 17β-HSD5·EM1404·NADP and 17β-HSD5·testosterone·NADP, the overall root mean square deviation value is 0.23 Å, but some local changes at the active site were significantly higher, as for the residue Pro-230 alone the Cα displacement is 2.9 Å. The side-chain conformation is also playing a role in the significant modification of the substrate binding pocket.

In various steroid hormones, including estrogens, androgens, and their precursors with the cyclopentenophenanthrene ring as the core, their modest structural alterations result in critical effects on their biological function (53, 54). The change in the binding site of 17β-HSD5 is very significant when compared with the binding site of 17β-HSD1. In the case of the latter it is a narrow hydrophobic tunnel, and its overall structure in the complex with estradiol is essentially the same as the native enzyme structure (root mean square deviation of 0.5 for all main-chain atoms) (45). The type 5 enzyme (17β-HSD5·AKR1C3) differs significantly from the type 1 enzyme by possessing a spacious and flexible steroid binding site. This is estimated to be ~960 Å³ or 470 Å³ in 17β-HSD5 ternary complex with testosterone or 4-dione, respectively, whereas being only 340 Å³ in 17β-HSD1·E2 complex (46). This volume in 17β-HSD1·

C, 17β-HSD5·testosterone·NADP, testosterone is colored in *brown*; and *D*, superimposition of 17β-HSD5·EM1404·NADP and 17β-HSD5·PEG·NADP complexes near the substrate entrance. The *blue dashed line* represents the Cα residues (131–133) in loop-C of 17β-HSD5·EM1404·NADP complex with weak electron density and thus not included in the final refined PDB coordinates. The *green dashed line* represents those un-modeled residues (127–137) in 17β-HSD5·PEG·NADP complex. Details are discussed in the text.
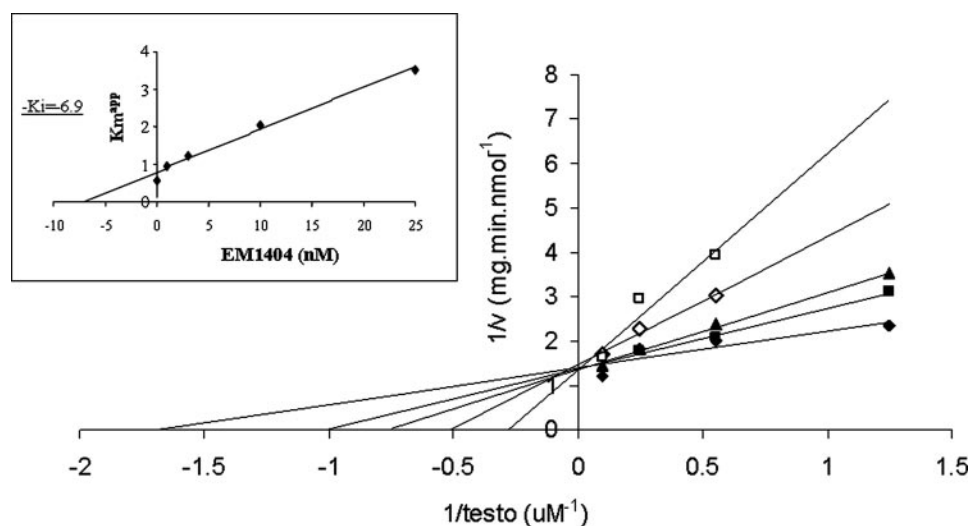
FIGURE 4. **Inhibition study on the conversion of testosterone to 4-dione by 17β-HSD5.** $1/v$ versus 1/[testosterone] in the absence or presence of various fixed concentrations of EM 1404. The experiment was carried out with EM1404 = 0 (◆), EM1404 = 1 nM (■), EM1404 = 3 nM (▲), EM1404 = 10 nM (◇), and EM1404 = 25 nM (□). The plot of apparent K_m versus [EM1404] inserted at *left top* shows the K_i value of EM1404: $(-K_i)$ is the intersection point on the [EM1404] axis, and a $K_i = 6.9 \pm 1.4$ nM was obtained.

testosterone complex is <2% different from that in 17β-HSD1·E2 complex.[5] This characteristic of the 17β-HSD5 binding site permits the docking of various steroids in different orientations, which in turn encompasses a wider range of activities from 20α-, 17β-, and 3α-HSD·KSR to prostaglandin 11-ketoreductase. In the ternary complex with testosterone the steroid C3–C17 position is quasi-reversed as compared with the complex with 4-dione. This multispecificity contributes significantly to steroid metabolism in peripheral tissues, due to the high levels of 17β-HSD5 mRNA in both breast and prostate tissues.

Using the 17β-HSD5·EM1404·NADP structure as a reference, eight other AKR1C3 complex structures were superimposed on the β-barrel motif. We observe how the conformations of four large loops move modestly to accommodate ligand binding in the substrate binding site (Fig. 3, *A–C*). Hydrogen bonding interaction is believed to be the key factor that selects the conformation of these substrates and inhibitors. For example, in the 17β-HSD5·4-dione·NADP complex (Fig. 3A), the O3 of 4-dione forms a hydrogen bond with Ser-129 hydroxyl (3.06 Å) that anchors loop-B (117–143) close to the substrate binding site. In this conformation the side chain of Phe-311 is pushed close to loop-B consequently leaving more space for the side chains of Trp-227 and Phe-306 to the position at the β-face of the steroid. As a result, the substrate binding pocket looks more compact (18). In the case of the 17β-HSD5·testosterone·NADP complex (Fig. 3B), hydrogen bonds at the two ends of the steroid determine testosterone orientations at the binding site (18). A similar interaction is observed in the AKR1C3·prostaglandin D_2·NADP complex, because the carbonyl O11 of prostaglandin D_2 participates in hydrogen bonding with Tyr-55 hydroxyl and His-117 Nε2 atom (20). The latter is involved in a hydrogen bond with a water molecule in a water channel, whereas the Tyr-55 hydroxyl par-

ticipates in a hydrogen bonding chain. It has also been reported that prostaglandin D_2 and rutin are involved in a similar hydrogen bonding network with AKR1C3, even though they have significantly different chemical structures (20).

The Binding of a Polyethylene Glycol Fragment in the Substrate-binding Site—While studying the enzyme-EM1404 interaction, we accidentally obtained a complex of PEG fragments in the substrate binding site in one of our crystal forms. This occurred early in our study while attempting to soak the inhibitor into the 17β-HSD5·NADP binary complex crystals with repeated additions of EM1404 but without success (see "Materials and Methods" and Figs. 1 and 3D)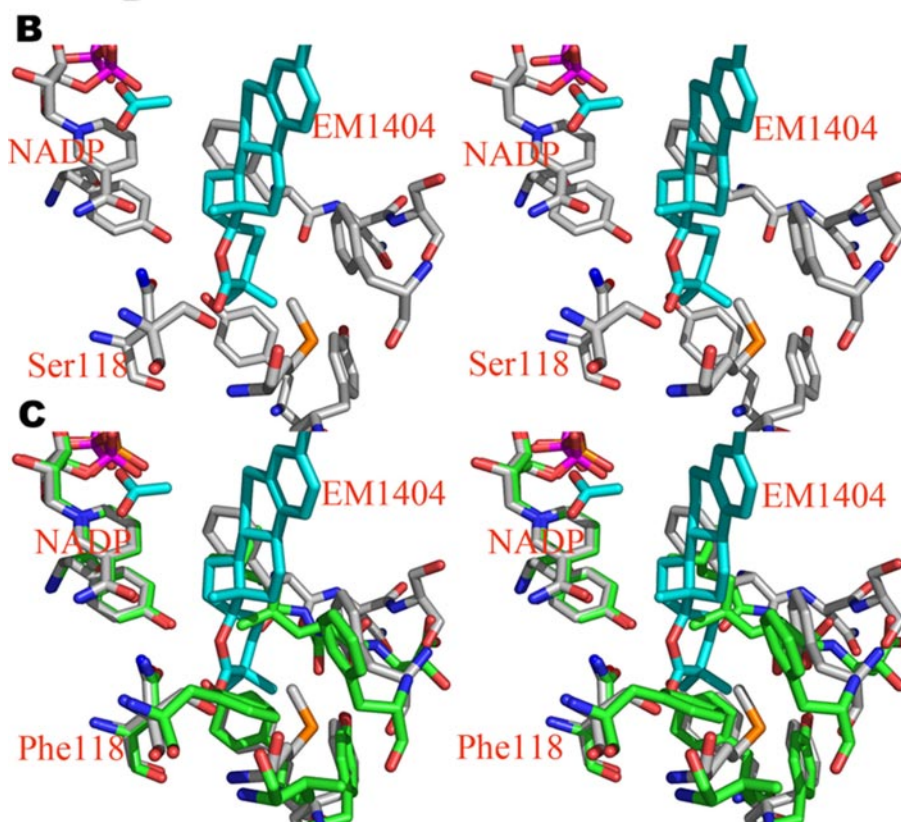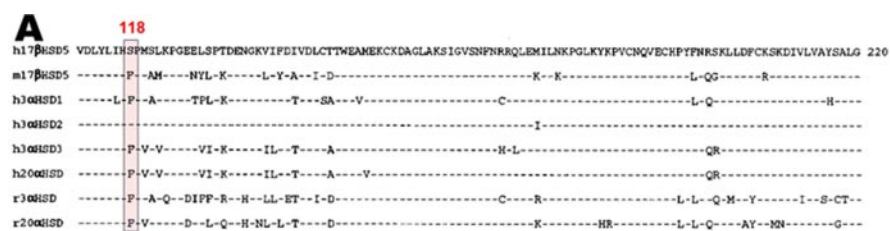. On the contrary, five ethylene glycol units can be identified with clear electron density at the bottom of the substrate binding site, whereas the sixth glycol unit near the entrance to the substrate binding site has less clear electronic density (the possible crystallization process can be found under "Discussion"). Compared with the 17β-HSD5·EM1404·NADP complex, the residues surrounding the substrate binding site have more free space to extend their side chains toward the center of the channel. The interactions between the enzyme and PEG are mostly hydrophobic; no hydrogen bonding interactions can be identified. In the final refined model we observed only the PEG fragment in the substrate binding site. Using the co-crystallization method (38), we obtained the ternary complex of 17β-HSD5·EM1404·NADP, and the main results have been described above. These two types of crystals have the same space group and very similar unit cells. We looked further into the crystal packing near the substrate entrance and found that the packing of loop-C indeed differs in both crystal forms (Fig. 3D). The electron density for loop-C is weak in both complexes but could be seen near the substrate entry path. A symmetry-related molecule is located near loop-C and may influence the location of loop-C at the entrance of the substrate binding site in both ternary complexes. The mechanism of these two crystallization methods is addressed in more detail under "Discussion."

17β-HSD Type 5 Inhibition by EM1404—As shown in Fig. 4, the Lineweaver-Burk plots for testosterone oxidation to 4-dione in the absence and the presence of different EM1404 concentrations intersect at the same point on the $1/v$ axis. For the reciprocal plots corresponding to different inhibitor concentrations, the curves in the presence of increasing inhibitor concentration result in a higher slope, pivoting around the intersection point on the control curve. This demonstrates a typical reversible and competitive inhibition, in agreement with Equation 1. The results also coincide with the inhibitor binding position in the substrate site shown by the crystallographic structure. A K_i

---

[5] W. Qiu and S.-X. Lin, unpublished results.
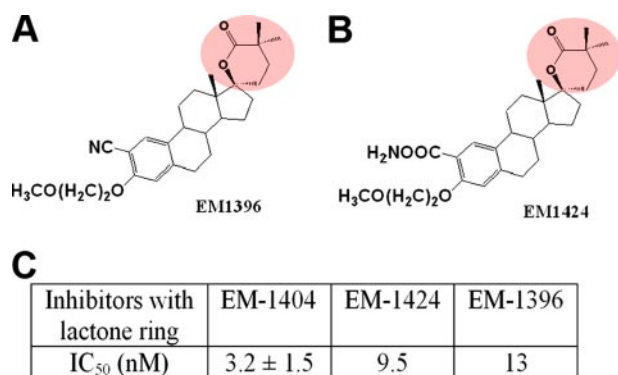
FIGURE 5. **Inhibition of 17β-HSD5 by different inhibitors with lactone ring.** EM1396 (*A*) and EM1424 (*B*) each have a lactone ring (marked in *pink*) next to the D-ring of steroid core, similar to EM1404. *C*, inhibition of 17β-HSD5 by these inhibitors (table adapted from Ref. 34) showing that the IC$_{50}$ for EM1404 is the smallest among these inhibitors. HEK cells were used as the enzyme source, using 0.1 μM [^{14}C]4-dione as the substrate in the essay. IC$_{50}$ values indicated the inhibitor concentration leading to 50% inhibition of the enzyme activity under the experimental conditions described in Ref. 34.

value of 6.9 ± 1.4 nM was calculated from the plot (Fig. 5) by the intersection of the above line on the left of the [I] axis, which was thus determined to be more than 40 times smaller than any other available inhibitor in the literature, demonstrating a strong enzyme inhibition by EM1404. The K_m of 17β-HSD5 for testosterone oxidation was determined as 2.9 ± 0.5 μM, suggesting EM1404 affinity is significantly higher than testosterone. Such an inhibition coincides well with the extensive interaction of EM1404 with the 17β-HSD5 binding pocket.

Comparison of Various Enzyme Inhibitors—Results from enzyme inhibition and molecular docking coincide with the fact that the lactone ring of EM1404 accounts for the strong interaction between the inhibitor and the enzyme. Those inhibitors with a lactone ring (*e.g.* EM1404, EM1424, and EM1396) have a higher affinity than testosterone (34). Our inhibition study is in coincidence with the structure-activity relationship of EM1404 carried out in the chemical screen (34), with the smallest IC$_{50}$ among all the available inhibitors for 17β-HSD·AKR1C3 (31–35). We docked these inhibitors into the crystal structure of 17β-HSD5-EM1404 complex using the Autodock program (49). It is interesting to point out that these inhibitors adopted a similar docking position with the lactone ring at the base of the binding pocket as observed for the 17β-HSD5·EM1404·NADP crystal structure (results not shown). By comparing the IC$_{50}$ for EM1404, EM1424, and EM1396 (Fig. 5), it appears that an amide group at the A-ring position contributes significantly to the higher affinity of EM1404 to 17β-HSD5 than the other inhibitors.

Structural Features of 17β-HSD Type 5 Pertinent to Inhibitor Design— A structure-based sequence alignment of several AKR family members revealed that only human 17β-HSD5 has a serine at position 118, whereas in other AKR members this position is occupied by a phenylalanine (Fig. 6*A*). In addition, the Ser-118 hydroxyl is engaged in a strong hydrogen bond (2.8 Å) with the 2'-carbonyl oxygen in the lactone ring of EM1404 (Figs. 2*A* and 6*B*). Superimposition of human 3α-HSD3 with human 17β-HSD5 in the inhibitor binding site shows that the bulkier side chain of Phe-118 in 3α-HSD3 will prevent the docking of the lactone ring of EM1404 to the bottom of the substrate binding site(Fig. 6*C*). We predict that this phenylalanine will obstruct any 17β-HSD5 inhibitor with a lactone

FIGURE 6. **Interaction of the lactone ring with Ser-118 in AKR1C enzymes.** *A*, the sequence alignment of several AKR1C family members. *B*, Ser-118 interaction with EM1404 in 17β-HSD5. Ser-118 hydroxyl forms a strong hydrogen bond (2.8 Å) with the 2'-carbonyl oxygen in the lactone ring. *C*, superimposition of human 3α-HSD3 with human 17β-HSD5 in the inhibitor binding site shows the steric hindrance from Phe-118 of 3α-HSD3 prevents the binding of the EM1404.

ring. Thus the lactone ring will ensure an additional specificity of inhibitors to the 17β-HSD5 enzyme.

Predictive Molecular Modeling and Dynamics—The above results did lead us to do inhibitor prediction theoretical studies using molecular modeling and dynamics as an extension of the present work (for more details, see supplemental materials).
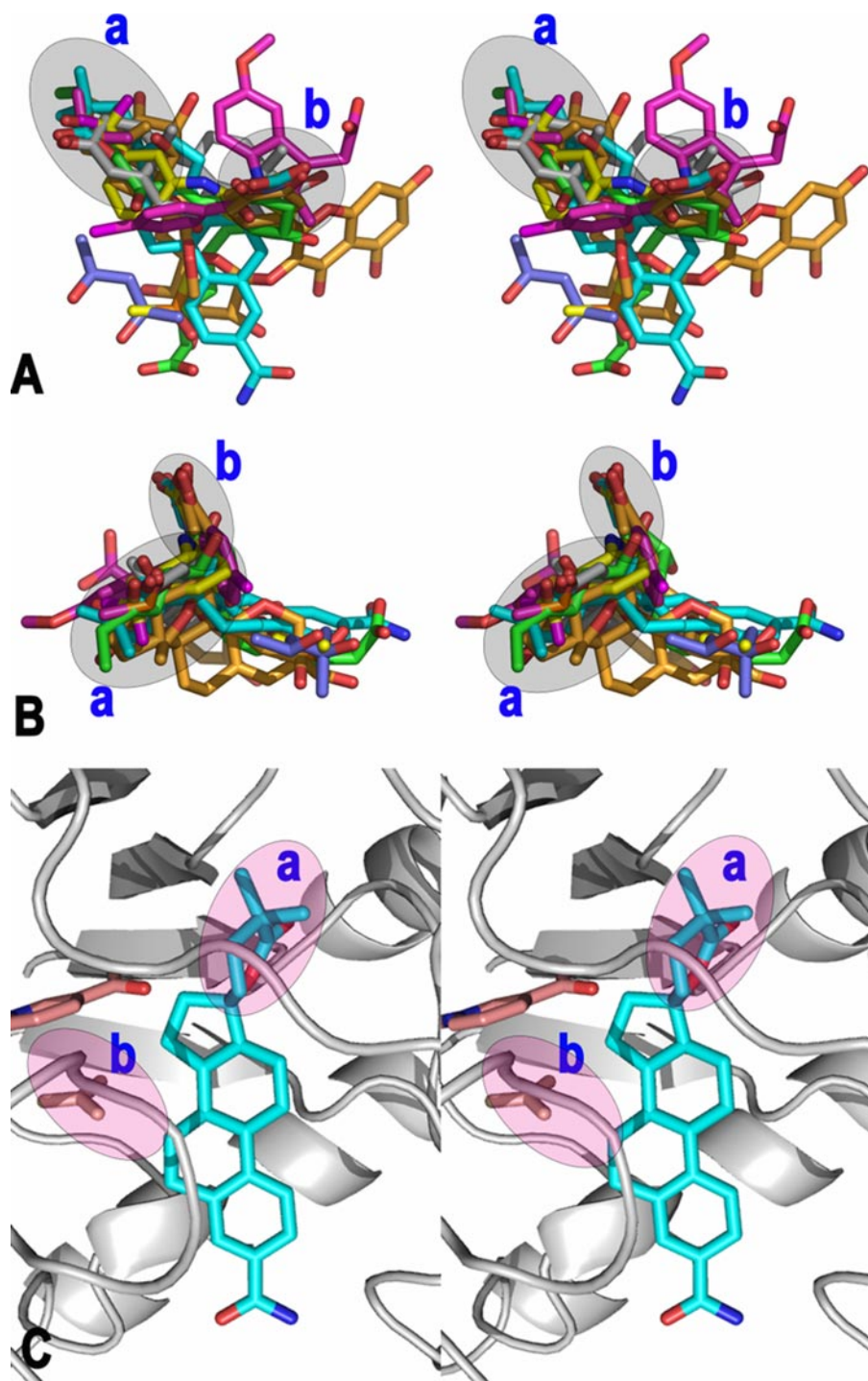

FIGURE 7. **Location of the sub-sites a and b in the binding site in 17β-HSD5·AKR1C3.** *A*, superimposition of different ligands in nine 17β-HSD5·AKR1C3 crystal structures (PDB code: 1S1R, 1S2A, 1S2C, 1RY0, 1RY8, 2FGB, 1Xf0, and 1AFS) using 17β-HSD5·EM1404·NADP (PDB code: 1ZQ5) as a reference on the triose-phosphate isomerase barrel motif. Using EM1404 as reference (colored in *cyan*), the top view of EM1404 showed two sites (*a* and *b*) as having high ligand occupancies (*shaded areas*), where *site a* corresponds to the lactone ring in EM1404 and *site b* is at the location of the acetate ion; *B*, view of the two sites perpendicular to *A*. *C*, location of the binding sites *a* and *b* relative to EM1404 in the 17β-HSD5·EM1404·NADP structure. NADP molecule is also shown near EM1404.

Firstly from the superimposition of nine liganded structures of the 17β-HSD5 binding site, we can identify two sub-sites in the binding site, namely sub-site a (for the binding of the lactone ring) and sub-site b (for the binding of the acetate), as having an elevated occupancy among the ligands (Fig. 7). Among those nine ligands only the flufenamic acid structure (Fig. 8B) occupies both sites. The structure of the 17β-HSD5·EM1404·NADP complex was superimposed with the 17β-HSD5·flufenamic acid·NADP complex, to examine the similarities between the bindings of the two ligands (Fig. 7A). We found that the carboxylate group of flufenamic acid occupies a similar position to the acetate ion in the HSD5·EM1404·NADP complex (*site b*, as described in Fig. 8), whereas the trifluoromethyl-benzene ring is situated near the position of the EM1404 lactone ring (*site a*, as described in Fig. 8). Based on this structural information, a new inhibitor is proposed by replacing the flufenamic acid trifluoromethyl-benzene ring by a lactone (Fig. 8B). The newly designed molecules were docked into the active site using the Autodock program. The predicted docking position is close to a position where all interactions with a residue are maximal (Fig. 8C).
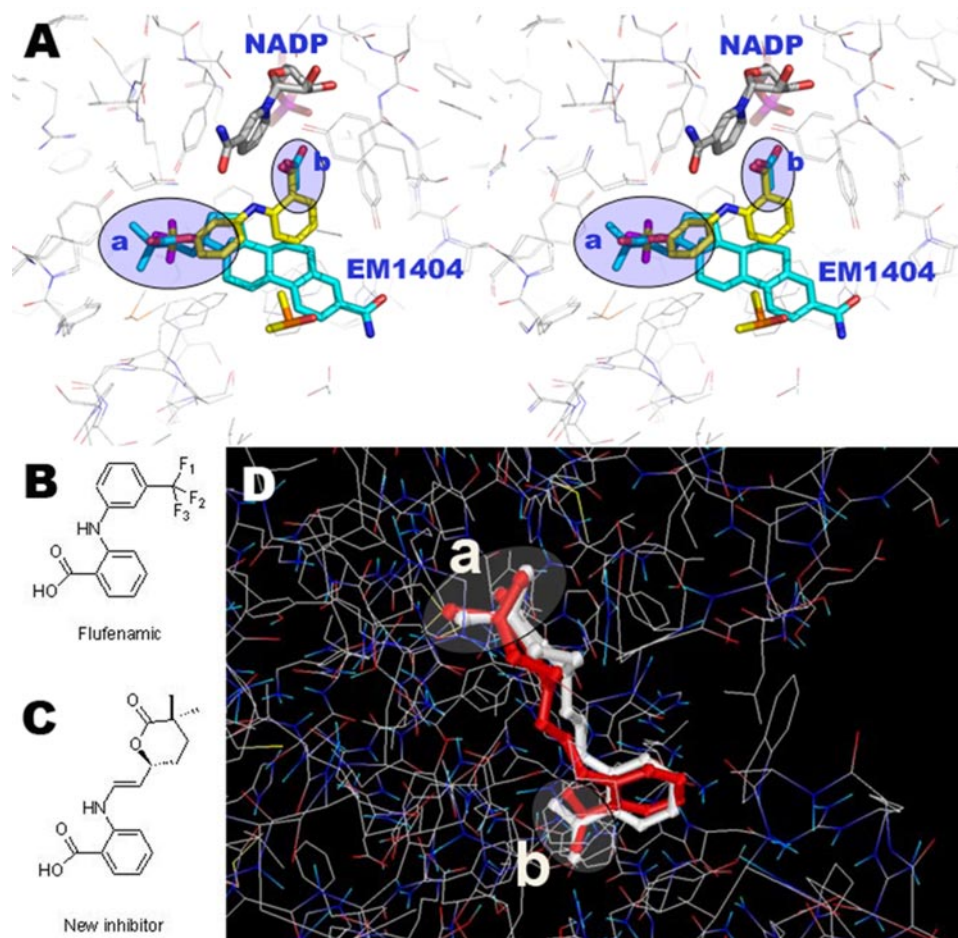
The fluctuation of the loop as observed by the molecular dynamics studies and principal component analysis (see supplemental material for more details) is much higher for the EM1404 complex than the new inhibitor complex, whereas the core protein movement remained the same. This suggests that the newly proposed inhibitor (Fig. 8C) has a potentially higher affinity compared with the EM1404.

DISCUSSION

EM1404, a potent inhibitor for 17β-HSD5 was first obtained from a chemical screen (34). Its high specificity toward the enzyme has been demonstrated by extensive interaction with 17β-HSD5 as shown by the 17β-HSD5·EM1404·NADP crystal structure. The new structural knowledge has in turn permitted further improvement of the inhibitor using molecular modeling. Thus

FIGURE 8. **Rational design of a new non-steroid inhibitor based on flufenamic acid.** *A*, superimposition of 17β-HSD5·EM1404·NADP complex with 17β-HSD5·flufenamic acid·NADP complex. *B*, chemical structure of flufenamic acid; *C*, chemical structure of a new inhibitor, obtained by the replacing the trifluoromethyl-benzene ring on the flufenamic acid with a lactone ring; *D*, the docking of the new inhibitor at the substrate binding site. The *white ball-and-stick model* represents the location of the new inhibitor derived from both 17β-HSD5·EM1404·NADP and 17β-HSD5·flufenamic acid·NADP complex structures, whereas the *red ball-and-stick model* is the real docking position for this new inhibitor obtained from Autodock. The locations of sites *a* and *b* are indicated with *circles* similar to what is shown in Fig. 7.

binding of those ligands/inhibitors are not stable or may have different conformations.

With the co-crystallization and soaking methods described under "Materials and Methods," two different structures, namely 17β-HSD5·EM1404·NADP and 17β-HSD5·PEG fragment·NADP were obtained (see "Results"). Using the established co-crystallization method for steroid enzymes with hydrophobic substrates or analogues, diluted enzyme-ligand solutions were gradually concentrated in the absence of PEG, permitting the full binding of the ligands into the hydrophobic sites, thus decreasing the free ligand concentration followed by the solubilization of additional steroid molecules into the solution in several cases. In fact, 17β-HSD1·estradiol complex solution at 300 μM (enzyme dimer) or 600 μM (steroid) was achieved (the stoichiometry was quantified using a radioisotope) leading to the high electronic density of estradiol in the binary complex (38). Another established method to obtain steroid complexes is the soaking method, making use of the high solubility of steroids or their analogues in a solution of PEG (a PEG solution with 0.5 or 0.8 mM steroids was able to be prepared and used for complex formation; refer to Refs. 47, 50, 51, and 52).

In the crystals obtained by soaking pre-formed 17β-HSD5·NADP crystals, PEG molecules may be introduced from the crystallization buffer while we prepared the binary complex crystals. We then attempted to soak the inhibitor EM1404 into this binary complex to form a ternary complex but did not succeed. For the 17β-HSD5·PEG fragment·NADP complex, this raises the question why PEG molecules cannot be replaced by EM1404, which is highly saturating the enzyme protein. The final concentration of EM1404 in the PEG solution was 560 μM, whereas the monomeric enzyme concentration is 330 μM in the crystallization solution for soaking as indicated under "Materials and Methods." In the crystal a symmetrically related molecule is located near loop-C and thus may force this loop to move closer to the entrance of the substrate binding site in the ternary complex of 17β-HSD5·PEG fragment·NADP (the *green dashed line* in Fig. 3*D*). It is likely that this blocks the exchange of PEG for EM1404 (Fig. 3*D*). In the 17β-HSD5·EM1404·NADP complex crystal obtained from co-crystallization, most residues in loop-C can be identified by its electron density (except for 131–133; see *blue dashed line* in Fig. 3*D*), and they are situated away from sub-

the present work demonstrates the advantage of a combined study of small molecule structure-activity relationship and protein structure-based drug design, both in the understanding of structure inhibition and the improvement of new inhibitors.

The structural explanation for the high affinity of EM1404 includes: (*a*) the contribution of a lactone ring at the D-ring to lower the binding energy; (*b*) the amide group at the A-ring end of EM1404 interacting with loop-A, loop-B, and loop-C; (*c*) the aromatic side chains of Trp-227, Phe-306, and Phe-311 form strong hydrophobic interactions between the enzyme and inhibitor, which stabilize loop-C and loop-D; (*d*) the plastic property of the binding pocket accommodates the shape of EM1404 (Fig. 1*C*). EM1404 and the acetate molecule occupy a very large volume of the binding pocket in this complex. Additional structural evidence for the stable binding of EM1404 is that, in the final model of the 17β-HSD5·EM1404·NADP structure, the average *B* factor of EM1404 model (10.5Å^2) is similar to that of its surrounding residues. In contrast, in the other complexes we described above, the *B* factor of the ligands/inhibitors is higher than the value of the surrounding residues, indicating that the

strate entry path. Of course, in the crystallization reported herein, the concentration of the steroid analogue has not been followed rigorously step by step as was done in the case of 17β-HSD1-estradiol (38), the alterative possibility of a solubility problem for EM1404 cannot be excluded for the unsuccessful formation of ternary complex from the enzyme-NADP binary complex crystals.

As mentioned above, one acetate molecule is defined at the catalytic site near the nicotinamide ring of NADP. This acetate molecule is believed to be introduced from the crystallization solution. Although the occupation of the acetate molecule at the substrate binding site does not interfere with EM1404 binding based on Autodock results, the binding energy of acetate can be used to develop a new inhibitor that could inhibit the enzyme more strongly. The CH3 group of the acetate is ~3.2 Å away from the B-ring of EM1404. To design an inhibitor that is more efficient than EM1404, a hybrid compound consisting of an acetate-like group and EM1404 could further increase its interaction and affinity with the enzyme, similar to the case of the hybrid inhibitor, EM1745, for 17β-HSD1 (51).

The substrate binding pocket is composed mainly of four flexible loops. We noticed that the volume of this pocket could be adjusted due to the modest flexibility of these loops. In one of our previous studied complex structures, the pocket size corresponds to the size of a steroid, such as 4-dione. In another case, it is significantly bigger than the corresponding steroid, thus allowing testosterone to adopt two distinct conformations (18). In an extreme case, the binding pocket can even tolerate a much bigger molecule, such as rutin (20). The stability of the substrate binding is heavily dependent on the conformation of these loops. For the future design of improved inhibitors, we can also focus on the A-ring end group by replacing the amide of EM1404 with a bulkier group that could potentially make more hydrogen bonding interactions with the protein side chains to stabilize these loops.

REFERENCES

1. Lopez-Otin, C., and Diamandis, E. P. (1998) *Endocr. Rev.* **19,** 365–396
2. Denmeade, S. R., Lin, X. S., and Isaacs, J. T. (1996) *Prostate* **28,** 251–265
3. Labrie, F., Dupont, A., Belanger, A., Giguere, M., Lacoursiere, Y., Emond, J., Monfette, G., and Bergeron, V. (1985) *J. Steroid Biochem.* **23,** 833–841
4. Pelletier, G., Luu-The, V., Tetu, B., and Labrie, F. (1999) *J. Histochem. Cytochem.* **47,** 731–738
5. Pelletier, G., Li, S., Luu-The, V., Tremblay, Y., Belanger, A., and Labrie, F. (2001) *J. Endocrinol.* **171,** 373–383
6. El-Alfy, M., Luu-The, V., Huang, X. F., Berger, L., Labrie, F., and Pelletier, G. (1999) *Endocrinology* **140,** 1481–1491
7. Labrie, F., Cusan, L., Gomez, J. L., Candas, B., Belanger, A., Luu-The, V., Labrie, C., and Simard, J. (2003) *Med. Sci.* (*Paris*) **19,** 910–919
8. Labrie, F., Dupont, A., Belanger, A., Cusan, L., Lacourciere, Y., Monfette, G., Laberge, J. G., Emond, J. P., Fazekas, A. T., Raynaud, J. P., and Husson, J. M. (1982) *Clin. Invest. Med.* **5,** 267–275
9. Labrie, F., Candas, B., Gomez, J. L., and Cusan, L. (2002) *Urology* **60,** 115–119
10. Lin, H. K., Jez, J. M., Schlegel, B. P., Peehl, D. M., Pachter, J. A., and Penning, T. M. (1997) *Mol. Endocrinol.* **11,** 1971–1984
11. Matsuura, K., Shiraishi, H., Hara, A., Sato, K., Deyashiki, Y., Ninomiya, M., and Sakai, S. (1998) *J. Biochem.* (*Tokyo*) **124,** 940–946
12. Burczynski, M. E., Harvey, R. G., and Penning, T. M. (1998) *Biochemistry* **37,** 6781–6790
13. Jez, J. M., Bennett, M. J., Schlegel, B. P., Lewis, M., and Penning, T. M. (1997) *Biochem. J.* **326,** 625–636
14. Jez, J. M., Flynn, T. G., and Penning, T. M. (1997) *Biochem. Pharmacol.* **54,** 639–647
15. Dufort, I., Rheault, P., Huang, X. F., Soucy, P., and Luu-The, V. (1999) *Endocrinology* **140,** 568–574
16. Lin, H. K., Steckelbroeck, S., Fung, K. M., Jones, A. N., and Penning, T. M. (2004) *Steroids* **69,** 795–801
17. Nakamura, Y., Suzuki, T., Nakabayashi, M., Endoh, M., Sakamoto, K., Mikami, Y., Moriya, T., Ito, A., Takahashi, S., Yamada, S., Arai, Y., and Sasano, H. (2005) *Endocr. Relat. Cancer* **12,** 101–107
18. Qiu, W. (2002) *X-ray Crystallographic Studies on Human Estrogenic Type 1 and Androgenic Type 5 17beta-Hydroxysteroid Dehydrogenases*, Ph.D. dissertation, Laval University, Quebec City, Quebec, Canada
19. Qiu, W., Zhou, M., Labrie, F., and Lin, S.-X. (2004) *Mol. Endocrinol.* **18,** 1798–1807
20. Komoto, J., Yamada, T., Watanabe, K., and Takusagawa, F. (2004) *Biochemistry* **43,** 2188–2198
21. Lovering, A. L., Ride, J. P., Bunce, C. M., Desmond, J. C., Cummings, S. M., and White, S. A. (2004) *Cancer Res.* **64,** 1802–1810
22. Wick, M., Hurteau, G., Dessev, C., Chan, D., Geraci, M. W., Winn, R. A., Heasley, L. E., and Nemenoff, R. A. (2002) *Mol. Pharmacol.* **62,** 1207–1214
23. Desmond, J. C., Mountford, J. C., Drayson, M. T., Walker, E. A., Hewison, M., Ride, J. P., Luong, Q. T., Hayden, R. E., Vanin, E. F., and Bunce, C. M. (2003) *Cancer Res.* **63,** 505–512
24. Rheault, P., Dufort, I., Soucy, P., and Luu-The, V. (1999) *Cytogenet. Cell Genet.* **84,** 241–242
25. Koh, E., Noda, T., Kanaya, J., and Namiki, M. (2002) *Prostate* **53,** 154–159
26. Bartsch, W., Greeve, J., and Voigt, K. D. (1987) *J. Steroid. Biochem.* **28,** 35–42
27. Martel, C., Rheaume, E., Takahashi, M., Trudel, C., Couet, J., Luu-The, V., Simard, J., and Labrie, F. (1992) *J. Steroid Biochem. Mol. Biol.* **41,** 597–603
28. Soronen, P., Laiti, M., Torn, S., Harkonen, P., Patrikainen, L., Li, Y., Pulkka, A., Kurkela, R., Herrala, A., Kaija, H., Isomaa, V., and Vihko, P. (2004) *J. Steroid Biochem. Mol. Biol.* **92,** 281–286
29. Oduwole, O. O., Li, Y., Isomaa, V. V., Mantyniemi, A., Pulkka, A. E., Soini, Y., and Vihko, P. T. (2004) *Cancer Res.* **64,** 7604–7609
30. Quinkler, M., Sinha, B., Tomlinson, J. W., Bujalska, I. J., Stewart, P. M., and Arlt, W. (2004) *J. Endocrinol.* **183,** 331–342
31. Krazeisen, A., Breitling, R., Moller, G., and Adamski, J. (2002) *Adv. Exp. Med. Biol.* **505,** 151–161
32. Penning, T. M., Burczynski, M. E., Jez, J. M., Lin, H. K., Ma, H., Moore, M., Ratnam, K., and Palackal, N. (2001) *Mol. Cell. Endocrinol.* **171,** 137–149
33. Bauman, D. R., Rudnick, S. I., Szewczuk, L. M., Jin, Y., Gopishetty, S., and Penning, T. M. (2005) *Mol. Pharmacol.* **67,** 60–68
34. Labrie, F., Belanger, A., Gauthier, S., Luu-The, V., Merand, Y., Poirier, D., Provencher, L., and Singh, S. M. (1999) *Inhibitors of Type 5 and Type 3 17beta-Hydroxysteroid Dehydrogenase and Methods for Their Use*, Canada PCT, WO99/46279
35. Krazeisen, A., Breitling, R., Moller, G., and Adamski, J. (2001) *Mol. Cell. Endocrinol.* **171,** 151–162
36. Zhou, M., Qiu, W., Chang, H. J., Gangloff, A., and Lin, S. X. (2002) *Acta Crystallogr. Sect. D Biol. Crystallogr.* **58,** 1048–1050
37. Penning, T. M., Burczynski, M. E., Jez, J. M., Hung, C. F., Lin, H. K., Ma, H., Moore, M., Palackal, N., and Ratnam, K. (2000) *Biochem. J.* **351,** 67–77
38. Zhu, D.-W., Azzi, A., Rehse, P., and Lin, S.-X. (1996) *J. Cryst. Growth* **168,** 275–279
39. Leslie, A. G. W. (1992) in *Joint CCP4 + ESF-EAMCB Newsletter on Protein Crystallography*, No. 26
40. Otwinowski, Z., and Minor, W. (1997) *Methods Enzymol.* **276,** 307–326
41. Kissinger, C. R., Gehlhaar, D. K., and Fogel, D. B. (1999) *Acta Crystallogr. Sect. D Biol. Crystallogr.* **55,** 484–491
42. Terwilliger, T. C. (2003) *Acta Crystallogr. Sect. D Biol. Crystallogr.* **59,**

38–44

43. Collaborative Computational Project Number 4 (1994) *Acta Crystallogr. Sect. D Biol. Crystallogr.* **50,** 760–763

44. Emsley, P., and Cowtan, K. (2004) *Acta Crystallogr. Sect. D Biol. Crystallogr.* **60,** 2126–2132

45. Azzi, A., Rhese, P. H., Zhu, D.-W., Cambpell, R. L., Labrie, F., and Lin, S.-X. (1996) *Nat. Struct. Biol.* **3,** 665–668

46. Lin, S.-X., Shi, R., Qiu, W., Azzi, A., Zhu, D.-W., Dabbagh, H. A., and Zhou, M. (2005) *Mol. Cell. Endocrinol.* **248,** 38–46

47. Qiu, W., Zhu, D.-W., Azzi, A., Campbell, R. L., Qi, H., Poirier, D., and Lin, S. X. (1999) *J. Steroid Biochem. Mol. Biol.* **68,** 239–244

48. Segel, L. A. (1976) *J. Theor. Biol.* **57,** 23–42

49. Morris, G. M., Goodsell, D. S., Halliday, R. S., Huey, R., Hart, W. E., Belew, R. K., and Olson, A. J. (1998) *J. Comput. Chem.* **19,** 1639–1662

50. Gangloff, A., Shi, R., Nahoum, V., and Lin, S.-X. (2003) *FASEB J.* **17,** 274

51. Qiu, W., Campbell, R. L., Gangloff, A., Dupuis, P., Boivin, R. P., Tremblay, M. R., Poirier, D., and Lin, S. X. (2002) *FASEB J.* **16,** 1829–1831

52. Breton, R., Housset, D., Mazza, C., and Fontecilla-Camps, J. C. (1996) *Structure* **4,** 905–915

53. Andersson, S. (1995) *J. Endocrinol.* **146,** 197–200

54. Han, Q., Campbell, R. L., Gangloff, A., Huang, Y.-W., and Lin, S.-X. (2000) *J. Biol. Chem.* **275,** 1105–1111

Structure-based Inhibitor Design for an Enzyme That Binds Different Steroids: A POTENT INHIBITOR FOR HUMAN TYPE 5 17 β-HYDROXYSTEROID DEHYDROGENASE

Wei Qiu, Ming Zhou, Mausumi Mazumdar, Arezki Azzi, Dalila Ghanmi, Van Luu-The, Fernand Labrie and Sheng-Xiang Lin

Access the most updated version of this article at doi: 10.1074/jbc.M606784200

Alerts:
- When this article is cited
- When a correction for this article is posted

Click here to choose from all of JBC's e-mail alerts

Supplemental material:
http://www.jbc.org/content/suppl/2006/12/14/M606784200.DC1

This article cites 51 references, 11 of which can be accessed free at
http://www.jbc.org/content/282/11/8368.full.html#ref-list-1